JOURNAL OF THERMOPHYSICS AND HEAT TRANSFER
Vol. 14, No. 2, April–June 2000

Impingement Heat Transfer on Dimpled Surfaces Using a Transient Liquid Crystal Technique

Gm. S. Azad,* Yizhe Huang,† and Je-Chin Han‡
Texas A&M University, College Station, Texas 77843-3123

Jet impingement heat transfer measurements are done for an array of inline air jets (four rows with each row having 12 jet holes) impinging orthogonally on dimpled (rough) target surfaces. Dimples 0.635 cm in diameter (equal to the jet diameter) and 0.3175 cm deep on the target surfaces are made in two different patterns ($23 \times 9 = 207$ dimples and $11 \times 5 = 55$ dimples) to make it a dimpled surface. Detailed measurements are done using a transient liquid crystal technique. Three different spent air crossflow orientations are studied. Measurements are done at four jet Reynolds numbers ranging from 4.85×10^3 to 1.83×10^4. The results show that the Nusselt numbers for a dimpled and a smooth surface are about the same. However, the dimpled surface provides a higher heat transfer due to an increased surface area when compared with a smooth surface. Similarly, the dimpled surface produces Nusselt numbers comparable to those of a pinned surface (a surface having pins of same size and number instead of dimples) for spent air crossflow orientations 2 and 3 but generates lower Nusselt numbers for orientation 1.

Nomenclature

A = heat transfer surface area
d = impingement jet hole diameter
h = local convection heat transfer coefficient, W/m$^2 \cdot$K
k = thermal conductivity of acrylic material
k_{air} = thermal conductivity of air
Nu = local Nusselt number, hd/k_{air}
$\overline{Nu}$ = span-averaged Nusselt number
Pr = Prandtl number
Re = average jet Reynolds number, $\rho V d/\mu$
T_i = initial temperature of the target surface
T_m = local bulk mainstream temperature of the flow
T_w = color change temperature of the liquid crystal, red to green
t = transition time for liquid crystal color change
V = average jet velocity
X = axial distance of the impingement target surface
Y = spanwise distance of the impingement target surface
Z = distance between jet plate and target plate
α = thermal diffusivity of acrylic material, and also jet inclination angle
μ = dynamic viscosity of air
τ = time step

Introduction

IMPINGEMENT with high-velocity gas jets is a common method of cooling, heating, or drying surfaces in a wide variety of process and thermal control applications. Heat transfer for impinging jets is generally higher than conventional methods. Thus, most practical applications of jet impingement occur in industries where high heating and cooling load is needed. Examples include cooling of gas turbine airfoils and electronic equipment, drying of paper and textiles, annealing of metals, and glass tempering operations. A two-dimensional array of impinging jets is also used to cool the midchord region of a gas turbine blade interior of an advanced gas turbine engine that operates at a high gas temperature (1300–1500°C). The jet air, after impingement, flows toward the rear of the blade through a channel formed between the jet orifice plate and the inner surface of the blade. In this configuration, impinging air from upstream jets imposes a confined crossflow to downstream jets. Thus, researchers investigate heat transfer and flow patterns for impinging jets that closely simulate a gas turbine airfoil internal cooling and combustion liner cooling applications.

Kercher and Tabakoff[1] investigated the effect of jet diameter, jet spacing, and jet-to-surface distance for a round air jet impinged on a flat surface. Florschuetz et al.[2] studied the effect of jet spacing, jet-to-surface distance, and crossflow for a two-dimensional array of circular air jets impinging on a flat surface. They also presented a correlation for inline and staggered hole patterns, including the effects of geometric parameters: streamwise hole spacing, spanwise hole spacing, and channel height to jet diameter ratio for one crossflow direction. Chupp et al.[3] evaluated the internal heat transfer coefficient for impingement cooling on the leading edge of a turbine blade. Bunker and Metzger[4] and Metzger and Bunker[5] also studied impingement cooling with and without film coolant extraction on the leading edge of a turbine airfoil. Van Treuren et al.[6] studied detailed heat transfer distributions under impinging jets. In an earlier paper, Huang et al.[7] also studied detailed heat transfer distributions on a smooth surface with different spent air crossflow orientations. All of these studies observed an increase in heat transfer with jet impingement and presented the effects of various geometrical and flow parameters on jet impingement heat transfer.

The cited data reported impingement jet heat transfer on smooth surfaces. However, jet impingement heat transfer on rough surfaces is important in many applications, including gas turbine blades. A surface may become rough from manufacturing process or a long service time, or roughness may be imposed intentionally to increase heat transfer performance. Haiping et al.[8] studied jet impingement heat transfer from a rib-roughened surface in the presence of an initial crossflow. They investigated the effect of the relative position of the jet hole to the ribs. They concluded that higher heat transfer values are obtained with jets impinging midway between the ribs compared with other locations. Chakroun et al.[9] studied jet impingement heat transfer on both smooth and rough surfaces. They investigated the roughness effect on impingement heat transfer. The roughness was composed of cubes of 1-mm dimension distributed uniformly along the plate. They did not present a detailed distribution, and the effect of different spent air crossflow orientation was not considered.

Trabold and Obot[10] studied impingement heat transfer on ribbed walls with different crossflow schemes. They measured the effect

Received 11 February 1999; revision received 12 March 1999; accepted for publication 24 November 1999.

*Research Assistant, Turbine Heat Transfer Laboratory, Department of Mechanical Engineering.
†Research Assistant, Turbine Heat Transfer Laboratory, Department of Mechanical Engineering; currently Mechanical Engineer, DSP Package Engineering, Motorola, Inc., Austin, TX 78735-8598.
‡Heat Transfer Research Institute Professor, Turbine Heat Transfer Laboratory, Department of Mechanical Engineering. Associate Fellow AIAA.

of geometrical and flow parameters on the heat transfer coefficient. They observed a small reduction in heat transfer coefficients in smaller X/d locations, but higher heat transfer coefficients in larger X/d locations for unidirectional crossflow scheme. They concluded that roughness elements (ribs) can compensate for the degradation in heat transfer usually associated with impingement crossflow on smooth surfaces. Gau and Lee[11] studied flow structure and heat transfer along ribbed walls impinging from a single slot air jet. They investigated the effect of rib heights, rib pitch-to-height ratio, slot width-to-rib height ratio, and nozzle to target wall distance. They concluded that heat transfer on ribbed surfaces are enhanced over a smooth surface. In a related study, Azad et al.[12] studied jet impingement heat transfer on a pinned surface with different crossflow orientations. They presented a detailed heat transfer coefficient distribution and concluded that jet impingement heat transfer coefficients on a pinned surface can be higher or lower than that on a smooth surface, depending on spent air crossflow direction.

It is a common practice to use a rough surface for heat transfer enhancement. A surface can be made rough in many different ways, for example, inserting ribs, pins, or making dimples on a surface. Ribs or pins are commonly used because many studies established that a rib-roughened or a pin-roughened surface enhances heat transfer coefficient. A dimpled surface may behave differently than a ribbed or a pinned surface under an impinging jet. Because a rib or a pin acts as a turbulator to the crossflow, it also disturbs the crossflow velocity. However, dimples may agitate the crossflow due to the ups and downs of the flowfield and may produce different heat transfer coefficients. A recent study by Chyu et al.[13] may support this phenomenon. They dealt with concavity-type dimples with convection and showed that dimples can enhance heat transfer, while the pressure losses were nearly one-half of the protruding elements. They used different dimple geometry from our studied dimple case. Schukin et al.[14] provided limited data downstream of the single concavity in a diffuser channel. Afnasyev et al.[15] experimentally studied the friction and heat transfer in a dimpled channel and reported a 30–40% heat transfer enhancement without any appreciable effect on the hydrodynamic loss. This study, however, was localized only at the midpoint (outside of concavity) of a staggered dimpled plate. Terekhov et al.[16] concentrated on the surface within a concavity and concluded the existence of an optimum concavity depth. Our study investigated a different dimple geometry than others, with three different crossflow orientations. Thus, the present study will fulfill the need for this additional heat transfer data on a dimpled target surface. This study also considers the effect of different spent air crossflow orientations on jet impingement heat transfer. Detailed heat transfer behavior on such a dimpled surface with different crossflow orientations under impinging jet is measured using a transient liquid crystal technique. Two different arrangements of dimples (many dimples and less dimples) on the target surface are studied. In the many-dimples case, the target surface has 9 rows with each row having 23 dimples ($9 \times 23 = 207$). Similarly, in the less-dimples case, the target surface has 5 rows with each row having 11 dimples ($5 \times 11 = 55$). Detailed heat transfer coefficient distribution data is collected for four different Reynolds numbers ranging from 4.85×10^3 to 1.83×10^4. The data for the less-dimples case are presented only for $Re = 9.55 \times 10^3$. The detailed heat transfer coefficient distribution results are presented and compared with smooth and pinned surface data.

Experimental Setup

Figure 1 shows the entire setup. The experimental setup consists of a computerized data acquisition system, an electric heater, an orifice plate, a diverter valve, a plenum, and the impingement test section itself. The computerized data acquisition system consists of a red–blue–green charge-coupled device camera, a computer with a frame grabber board, and a video monitor. The camera focuses on the liquid crystal-coated test surface and catches the color signals during the thermal transient test. The camera splits the color signal into red, green, and blue and passes the signals to the frame grabber board in the computer. The frame grabber board is programmed to analyze the color change using an image processing software. The

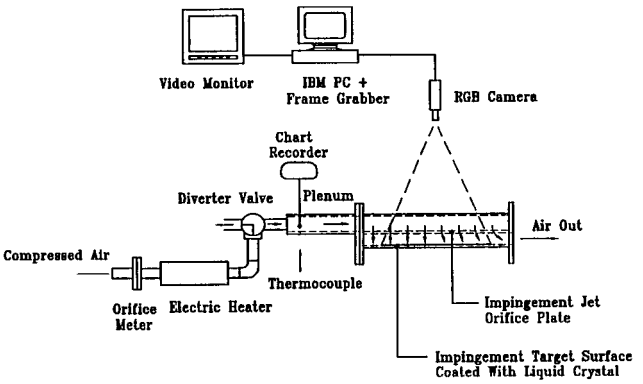

Fig. 1 Schematic of the experimental setup.

video monitor works as a reference to adjust the camera focus. The software analyzes the picture frame by frame for a color change. The analysis records the time of transition of the liquid crystal color change from the initial colorless state to the onset of green during the transient test. We used a lighting intensity threshold method. This method requires a background lighting intensity correction. This ensures that all of the points in the region of interest are at a lower intensity than the color change transitional intensity. The high resolution of the technique provides detailed distribution data at each point on the surface, which cannot be achieved by multiple thermocouples.

The inline air heater controls the required airflow rate and heats up the air to a preset temperature. The three-way ball diverter valve routes the air away from the test rig when no test is in progress. The orifice plate measures the steady-state airflow rate, and a strip chart recorder measures the mainstream flow temperature from a thermocouple during the transient test. The test section consists of two compartments joined by a jet plate having an array of jet holes of diameter 0.635 cm. The top compartment is a pressure chamber, whereas the bottom compartment is the impingement channel. The plenum is a 91.44-cm-long chamber through which the flow develops before entering to the pressure chamber. The jet plate thickness is equal to the jet hole diameter. The plate has 4 rows of holes, each row has 12 holes through the length of the plate. The jet-to-jet spacing is four times the hole diameter ($X/d = Y/d = 4$). The length of the test section is 30.48 cm. The inlet pressure chamber has a cross-sectional area of 12.7×2.54 cm, and the impingement channel has a cross-sectional area of 12.7×1.905 cm. The distance between the jet plate and the impingement target surface is three times the jet hole diameter ($Z/d = 3$).

Because the study focuses on a dimpled surface, a typical jet plate geometry is selected. The target surface has a constant cross section of 30.48×12.7 cm. Dimples of 0.635 cm in diameter (equal to the jet diameter) are fabricated in different patterns on the target surfaces. In one case (many-dimples case) 9 rows of dimples with each row having 23 dimples ($23 \times 9 = 207$) are made on the target surface. Similarly, the other case has 5 rows of dimples with each row having 11 dimples (11×5), machined on the target surface. In both cases, the dimple depth below the target surface is 0.3175 cm. The test section is made of clear acrylic material. The impingement target surface is made from black acrylic sprayed with liquid crystals on the inside surface. The dimples are also sprayed with liquid crystals. However, the heat transfer data are taken only on the bottom surface of the dimples and the impingement target surface between the dimples. The data on the peripheral surface of the dimples are not considered for heat transfer coefficient calculations. This peripheral surface is about 33.8 and 9% of the total projected surface area for the many- and the less-dimples cases, respectively.

Figure 2 shows the target surfaces with three different exit flow direction for the many-dimples case. The three flow directions are obtained by changing the discharge openings. The orientations provide three different crossflow effects created by the spent jets exiting out of the impingement channel. Figure 3 shows the target surface for the less-dimples case, the jet plate, and an enlarged view of a

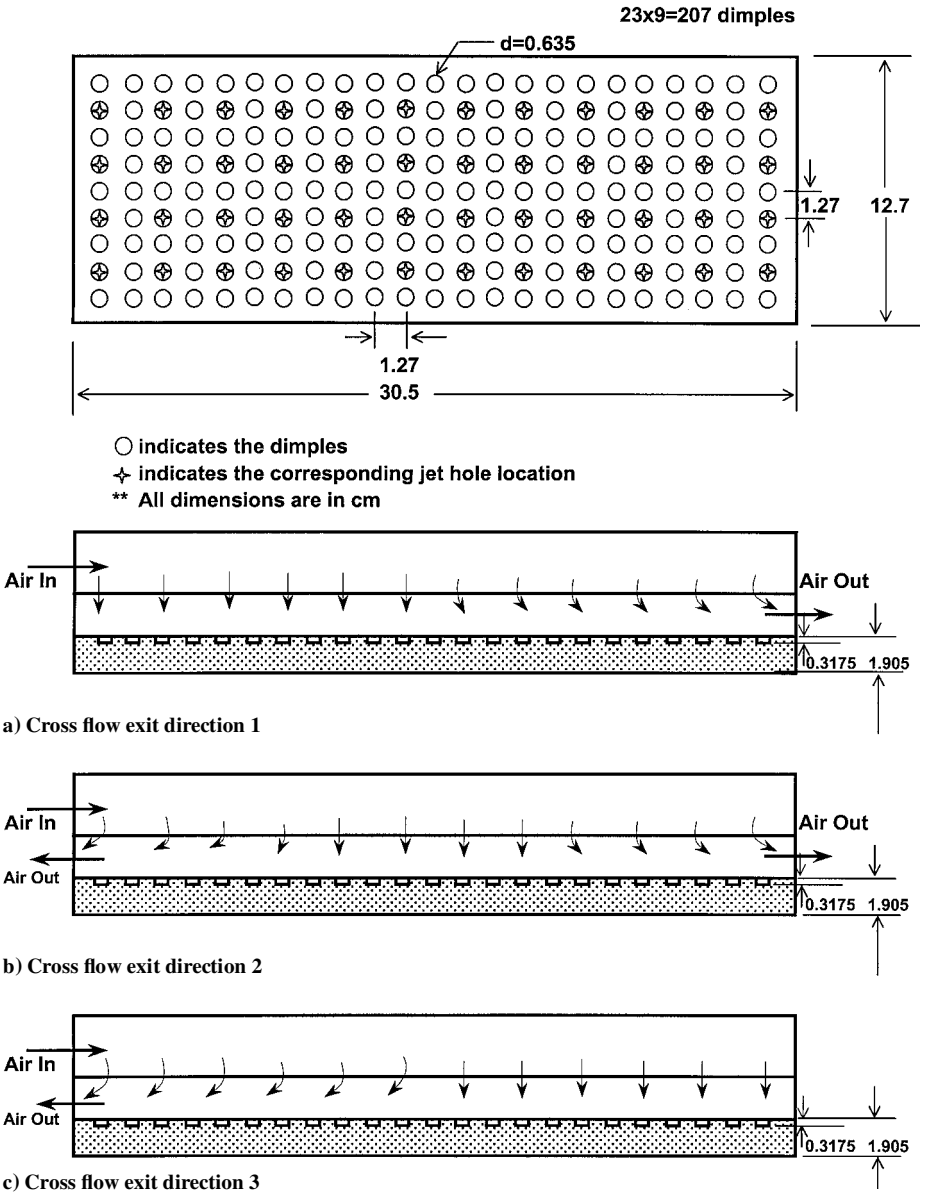

Fig. 2 Impingement target surface with different exit flow direction (many-dimples case).

dimple in the target plate. The dimple is machined into the target surface. The edges are kept as they are; no chamfering or any other treatment is done.

Theory and Test Procedure

Liquid crystal is sprayed over the target surface, and the test section is assembled according to the desired exit flow orientation. The camera is set up and focused on the target surface. A threshold intensity method of transient liquid crystal technique is used. This method requires a background intensity correction based on the lighting conditions on the region of interest (ROI). This ROI is our data collection region. This background light intensity correction ensures that all of the points in the ROI are at intensity lower than the real color change transition. Our test surface is kept at a room temperature, and heated air is introduced through the test section. Each test run is a thermal transient initiated by the sudden introduction of heated air into the test section, which results in a color change of the surface liquid crystal coating. Heated air is diverted away from the test section at the beginning of every test run so that the channel walls remain at the laboratory ambient temperature. The valve remains in the diverted position until steady flow and a preset temperature have been achieved in the diversion flow loop. The valve is then switched to route the hot air into the test section. Accurate and coordinated measurement of air temperature and the color change time is very important for reliable data. To reduce any measurement uncertainty, the automated computer data acquisition program and the chart recorder are simultaneously switched on to measure the color change (from red to the onset of green) transition time and temperature data. A typical air temperature is about 50°C, the initial temperature of the target plate is 24°C, the liquid crystal color change (from red to the onset of green) temperature is 32.7°C, and the color change time ranges from 10 to 40 s throughout the surface. Each test is repeated to check data repeatability. The data acquisition system transfers the data into a matrix of color change time over the entire surface. A computer program calculates the local heat transfer coefficient from the time and temperature data.

The test condition is assumed to be a one-dimensional transient conduction model through a semi-infinite solid with surface convection. The following equation describes the surface temperature:

$$\frac{T_w - T_i}{T_m - T_i} = 1 - \exp\left(\frac{h^2 \alpha t}{k^2}\right) \operatorname{erfc}\left(\frac{h\sqrt{\alpha t}}{k}\right) \tag{1}$$

where T_i(~24°C), T_m(~50°C), t(~10–40 s), T_w(32.7°C), k, and $\alpha(k/\rho c)$ of the solid are known and h is unknown. Note that the target surface is made of acrylic, which has a very low thermal conductivity (~0.18 W/m K). The test duration is smaller than the

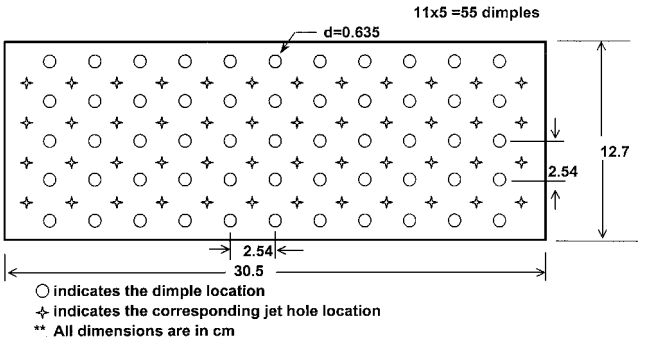

a) Target surface for less-dimples case

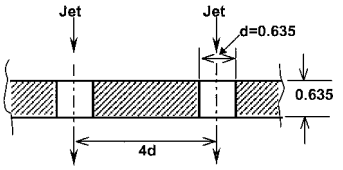

b) Jet plate

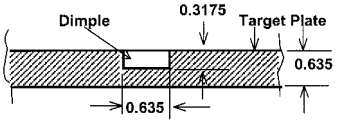

c) Enlarged view of a dimple in the target plate

Fig. 3 Target surface for less-dimples case, the jet plate, and a dimple.

time required for the temperature to penetrate the full thickness of the insulating acrylic material. The time for the color change transition is captured at the surface, which was initially at a uniform room temperature. Thus, we can consider a one-dimensional semi-infinite solid assumption. This assumption is even valid near the corners of the dimples except the exact corner edge. The heat transfer coefficient h can be calculated from Eq. (1).

The mainstream air is heated to a preset temperature (50°C), which makes the color change time from 10 to 40 s. The chart recorder measures the gradual change of the mainstream temperature during the transient test. The mainstream temperature is measured at the inlet of the pressure channel. However, we need to know the temperature of the air immediately before impingement. The mainstream temperature cannot be represented as a single step change. Because the mainstream temperature depends on time, the solution represented by Eq. (1) must include the gradual change of the temperature. The time history of the mainstream air temperature is reproduced as a series of step function, and then using Duhamel's superposition theorem, the solution in Eq. (1) is represented as

$$T_w - T_i = \sum_{j=1}^{N} \left\{ 1 - \exp\left[\frac{h^2 \alpha (t - \tau_j)}{k^2} \right] \times \operatorname{erfc}\left[\frac{h\sqrt{\alpha (t - \tau_j)}}{k} \right] \right\} [\Delta T_{mj}] \quad (2)$$

where ΔT_{mj} and τ_j are the temperature and time step changes from the chart recorder output. Equation (2) is solved to obtain the local heat transfer coefficient at every point on the measured region (250×100 points). The uncertainty in the Nusselt number, estimated by the method of Kline and McClintock,[17] is ±5.9%.

Results and Discussion

Several flow and geometrical parameters affect jet impingement heat transfer. The jet impingement Nusselt number can be represented as a functional form of these parameters as

$$Nu = (hd/k_{\text{air}}) = f[Re, Pr, (X/d, Y/d, Z/d, \alpha), \text{surface condition, flow orientation, etc.}] \quad (3)$$

where Reynolds number Re and Prandtl number Pr are flow parameters, and jet spacing to diameter ratio (X/d, Y/d), jet plate to target plate distance to diameter ratio (Z/d), and the jet inclination angle α are the geometric parameters. The target surface condition and the flow exit orientation are important parameters that have a significant effect on impingement heat transfer. This work studies the effect of a dimpled surface (target surface condition) with different spent air crossflow orientations on local heat transfer from impinging air jet. The heat transfer data are collected and presented for Reynolds numbers ranging from 4.85×10^3 to 1.83×10^4. The results are presented for different crossflow orientations. Detailed local heat transfer coefficients and span-averaged Nusselt number distributions are presented, and the results are compared with existing data.

Detailed Local Heat Transfer Coefficients

The local Nusselt number distributions as shown in Figs. 4–6 are presented as a function of nondimensional location X/d and Y/d. The results are presented from $X/d = 3.5$ to 44.5 in the streamwise direction over the entire span. Results shown in the detailed distribution correspond to the 10 central jet row locations out of the 12 jet rows of the plate. Results corresponding to the two end rows are not shown in the distributions. The jet mass flow distribution pattern is helpful to interpret the heat transfer results. In an earlier related study by Huang et al.,[7] the pressure distribution and the corresponding jet mass flow were measured for the same flow condition with a smooth target surface instead of a dimpled surface. The results show that the jet mass flow rate jumps from first hole location to the second hole location and then slightly increases toward the higher X/d for crossflow orientation 1, whereas it slightly increases from first jet hole toward the higher X/d for orientation 2. However, it remains almost constant for orientation 3. The maximum variation of jet mass flow rate occurs for orientation 1, and the variation is about ±6% from its average value. The same jet plate and the pressure chamber are used for this dimpled surface. We expect an approximately similar jet flow distribution patterns in this dimpled case.

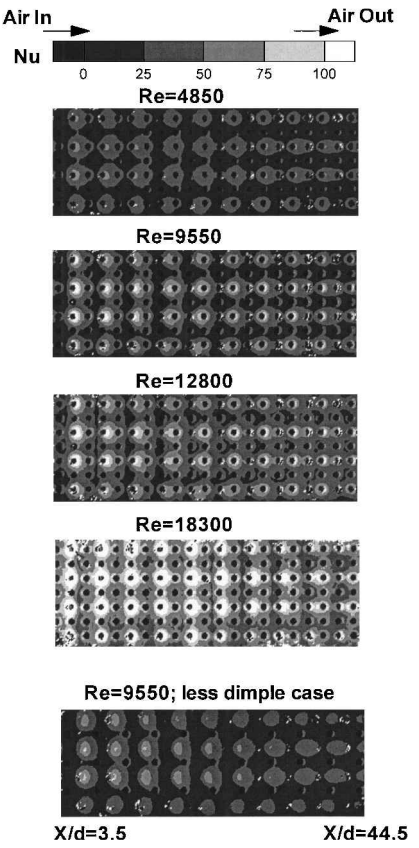

Fig. 4 Detailed Nusselt number distributions for orientation 1.

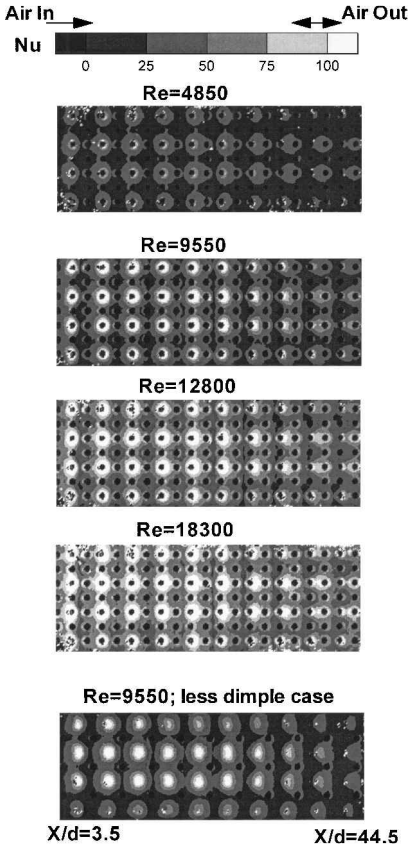

Fig. 5 Detailed Nusselt number distributions for orientation 2.

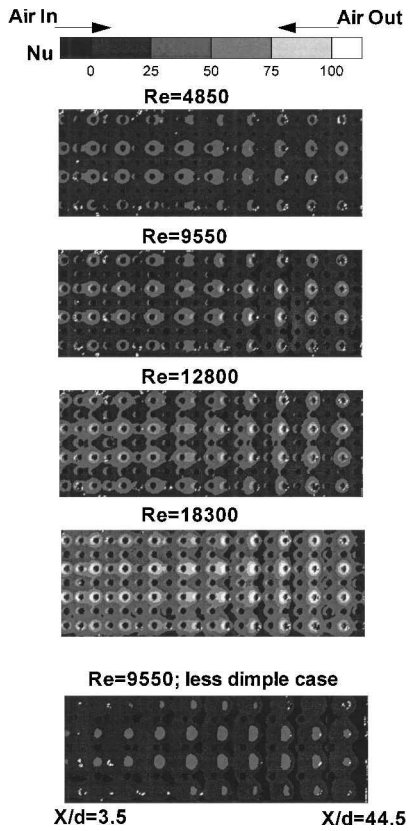

Fig. 6 Detailed Nusselt number distributions for orientation 3.

Figure 4 presents the local detailed distributions for flow orientation 1. In this orientation, the flow enters the pressure chamber at one end ($X/d = 0$) and exits the impingement channel on the other end ($X/d = 48$). The flow enters and exits in the same direction. The result show that the local heat transfer coefficient increases with an increase in the jet Reynolds number. The heat transfer coefficient slightly decreases as X/d increases. The portions of the surface that are directly under the jets (jet spots) have higher heat transfer coefficients than the neighboring space. In the many-dimples case, the jets directly impinge on some dimples. Thus, those dimples have higher heat transfer coefficients than the neighboring dimples. However, in the less-dimples case, the jets impinge on the surface between dimples. Thus, those jet spots have higher heat transfer coefficients than neighboring space and dimples. The jet air, after impingement, passes over the dimpled surface as a crossflow. While passing over the dimples, the disturbance of the crossflow created by the dimples only increases the heat transfer coefficient slightly. The amount of spent air crossflow increases with increasing X/d. Toward higher X/d, the strong crossflow velocity deflects the jets. Thus, the jets cannot penetrate to the target surface. Therefore, the local heat transfer coefficient decreases in the exit flow direction (at higher X/d).

Figure 5 shows a detailed distribution for flow orientation 2. In this orientation, the flow enters the pressure chamber at one end ($X/d = 0$) and exits at both ends. The highest local heat transfer coefficients are at the midportion of the surface, where the jets impinge normally. The heat transfer coefficients around the edges of the dimples are also higher due to a thinner boundary layer around the edges. At both ends, the heat transfer coefficient decreases slightly because the crossflow deflects the jets and the jets cannot penetrate into the target surface. This decrease in heat transfer coefficient is prominent at higher X/d than at lower X/d. This happens because of a stronger crossflow at higher X/d because the flow enters the pressure chamber at $X/d = 0$ toward a direction of higher X/d. Thus, the crossflow velocity is stronger at higher X/d even though the flow exits in both higher and lower X/d directions.

Figure 6 shows the detailed distributions for flow orientation 3. In this orientation, the flow exits in the opposite direction of the flow entrance. This means that the flow exits and enters at $X/d = 0$. The local heat transfer coefficients are relatively small compared with the other two flow orientations. In this orientation, most of the spent air exits easily through the exit end (see Fig. 2c) and does not possess a longer distance of crossflow. At higher X/d, the spent air crossflow is minimum, and the amount of spent air crossflow increases toward lower X/d. Because of this higher mass flow rate, the crossflow velocity also increases with decreasing X/d. Thus, the jets cannot penetrate the surface due to this strong crossflow effect, which results in a decrease in the heat transfer coefficient at lower X/d.

The jet Reynolds number has similar effect on jet impingement heat transfer for all three flow orientations. An increase in jet Reynolds numbers from 4.85×10^3 to 1.83×10^4 increases the local heat transfer coefficient throughout the target surface.

Span-Averaged Nusselt Number Distributions

Figure 7 shows the jet Reynolds number effect on span-averaged Nusselt number distributions with three exit flow orientations for the many-dimples case. In every orientation, the Nusselt numbers increase with an increase in jet Reynolds number. The Nusselt numbers decrease toward the exit direction in all three crossflow orientations. A strong crossflow when passed over the dimples enhances the heat transfer coefficient. However, a strong crossflow deflects the jets and prevents the jets from impinging the target surface. An impinging jet always predominates over the crossflow effect for heat transfer enhancement. Thus, a stronger crossflow toward the exit direction deflects the impinging jets. It prevents the jets impinging the target surface, which results in a slightly lower heat transfer coefficient toward the exit direction for all three exit orientations, as also happened for a smooth surface case as shown by Huang et al.[7] In flow orientation 2, this decrease is prominent at higher X/d even though the flow exits in both higher and lower X/d direction. In flow orientation 3, this decrease in the exit direction (lower X/d)

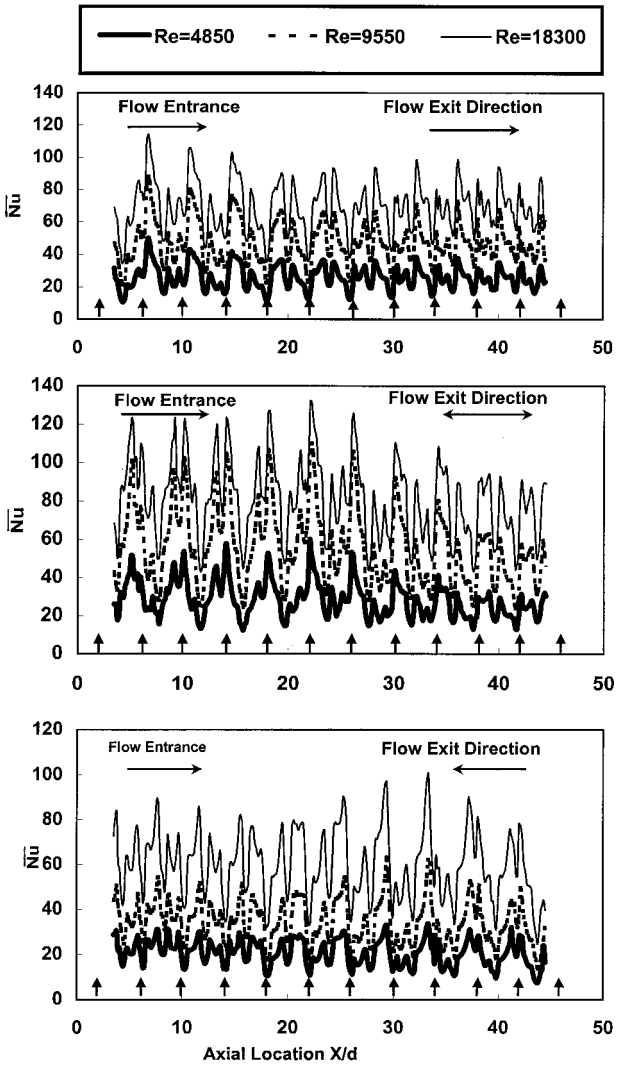

Fig. 7 Effect of Reynolds number on span-averaged Nusselt number (many-dimples case).

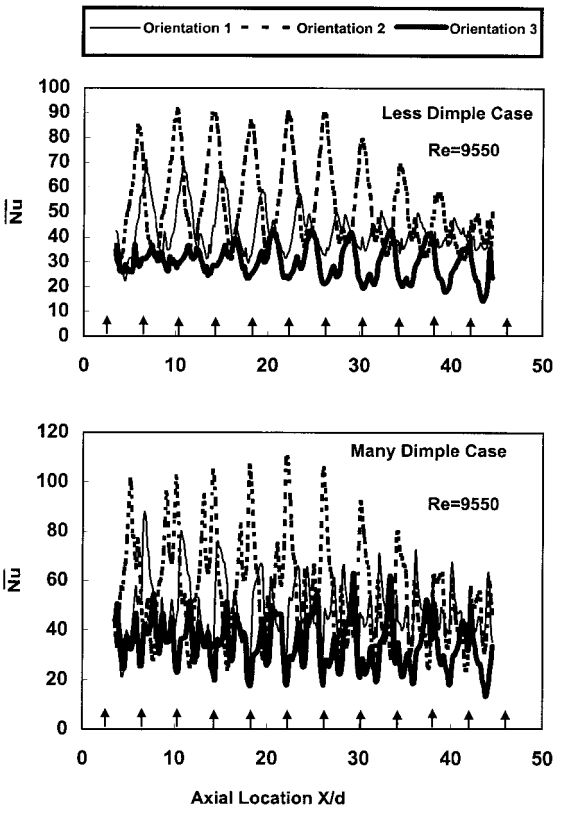

Fig. 8 Span-averaged Nusselt number as a function of exit flow direction ($Re = 9.55 \times 10^3$).

is very small. The arrows at the bottom of each Fig. 7 part indicate the impinging jet hole locations. The peaks in Figs. 7 correspond to jet impingement and dimple locations. The peaks corresponding to jet impingement locations have higher Nusselt number values than those at dimple locations. The jet hole and the jet impingement locations should match, as happened for midsection of exit orientation 2, where the flow exits in both directions, as seen in the second part of Fig. 7. However, the jet impingement locations are shifted (as the jets are deflected) from the jet hole locations due to the crossflow effect, as seen for orientations 1 and 3, and toward the exit ends of orientation 2. The impingement locations shifted toward higher X/d for orientation 1 because the crossflow exits in that direction. Similarly, the impingement locations shifted toward lower X/d for orientation 3 because the crossflow exits in that direction.

Figure 8 shows the flow orientation effect on span-averaged Nusselt numbers for $Re = 9.55 \times 10^3$. Flow orientations 1 and 2 provide higher heat transfer coefficients compared to orientation 3 for both cases (many-dimples and less-dimples cases). In orientation 3, most of the spent air exits easily through the exit end, and the impinging jet mass flow rate is smaller toward the higher X/d location, compared with the other two orientations. Because the crossflow exit direction is opposite to the flow direction in the pressure chamber, the overall flowfield in the impingement channel may be retarded. This results in a lower heat transfer coefficient. Flow orientation 2 provides the highest heat transfer coefficient for both the many- and less-dimples cases. It is clear from the less-dimples case that the jet impinges normally on the target surface for orientation 2. However, the jet is deflected toward right for orientation 1 and toward left for orientation 3 due to the crossflow effect. Thus, the Nusselt number peaks also shifted toward the right and the left from the jet hole location for orientations 1 and 3, respectively.

Comparison with Existing Data

The results are compared with some smooth and rough surface data that are available in the existing literature. Detailed heat transfer coefficient distributions from this study are averaged over the entire target surface to get a single value for each Reynolds number and each orientation. Note that the heat transfer data are collected only on the bottom surfaces of the dimples and the smooth target surface between dimples. The data from the peripheral surface of the dimples are not considered here. This peripheral area is 33.8 and 9% of the total projected surface area for the many-dimples and the less-dimples cases, respectively. The heat transfer coefficient on this peripheral area could be higher or lower. Whatever the value is, this increased area will further increase the total heat transfer from the dimpled surface because this is an additional surface area. However, the total averaged (when this peripheral area is considered) heat transfer coefficient or the Nusselt number could be lower or higher than the presented value depending on the heat transfer coefficient of this peripheral area. The averaged Nusselt numbers for each orientation are plotted as a function of Reynolds number to compare with the existing data as shown in Figs. 9 and 10. The present data without the peripheral surface data correlate with the Reynolds number dependence as $Nu = 0.049Re^{0.74}$, $0.029Re^{0.82}$, and $0.023Re^{0.8}$, for orientations 1, 2, and 3, respectively.

Figure 9 compares the same three spent air crossflow orientations in this study on dimpled surfaces and an earlier related study on a smooth surface by Huang et al.[7] The correlation developed by Kercher and Tabakoff[1] is also included for comparison. The smooth surface result of Huang et al.[7] reveals that flow orientation 2 provides the highest heat transfer coefficient over the entire surface, whereas flow orientation 3 provides the lowest. The heat transfer coefficient for flow orientation 3 might be lower because of the exit

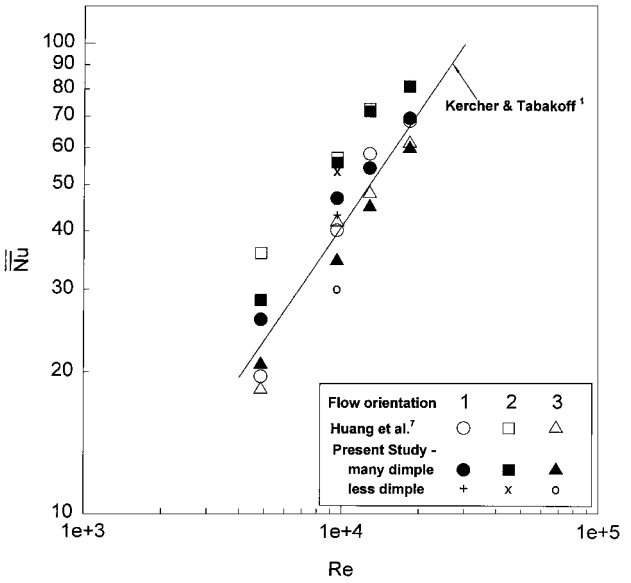

Fig. 9 Comparison of averaged Nusselt number with smooth surface data.

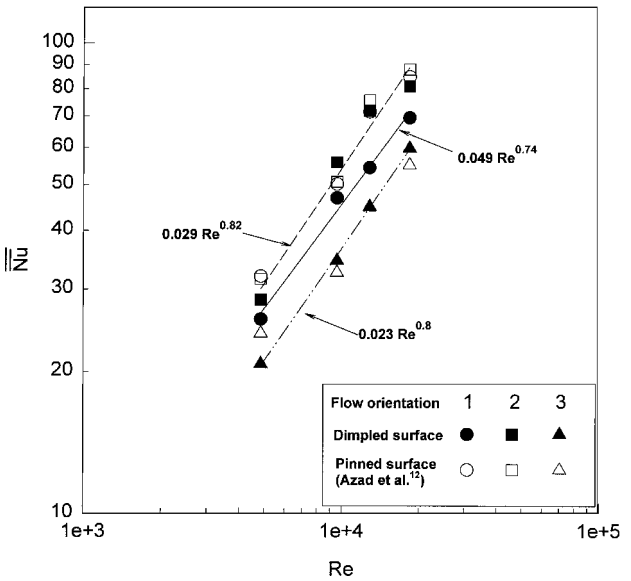

Fig. 10 Comparison of averaged Nusselt number with pinned surface data.

of the impingement channel being on the same side as the inlet to the pressure chamber. Smooth surface data of Huang et al. for orientation 1 and Kercher and Tabakoff's[1] correlated data are about the same. The crossflow effect in Kercher and Tabakoff's study is similar to that for flow orientation 1 in the Huang et al.[7] study.

This study uses similar geometrical parameters, X/d, Y/d, and Z/d, and spent air crossflow orientations as used in the Huang et al.[7] study, except the smooth target surface is replaced by the dimpled one. The dimpled surface Nusselt numbers for orientations 1 and 2 are higher than orientation 3. In orientation 3, most of the spent air exits easily and does not posses a longer distance of crossflow because the exit end is on the same side of the flow entrance in the pressure chamber. These results when compared with smooth surface data of Ref. 7 reveal that the Nusselt numbers for the dimpled surface (many-dimples case) are higher than the smooth surface at low Reynolds numbers but about the same at high Reynolds numbers for orientation 1. The Nusselt numbers for both cases are about the same for orientation 2 except at $Re = 4.85 \times 10^3$ the Nusselt number for the smooth surface is higher. Similarly, for orientation 3, the Nusselt numbers for the dimpled surface (many-dimples case) and the smooth surface are about the same. For the less-dimples case, the Nusselt numbers are obtained at only one Reynolds number ($Re = 9.55 \times 10^3$), and the Nusselt numbers are lower than for the many-dimples case.

The Nusselt numbers for the many-dimples case in flow orientations 1 and 2 are higher than the correlated results of Kercher and Tabakoff.[1] This result demonstrates that crossflow has a stronger effect on the heat transfer coefficient. Nusselt numbers for a smooth surface and a dimpled surface are about the same; however, a dimpled surface can provide higher heat transfer than a smooth surface due to an increased surface area as compared to a smooth surface case. A dimpled surface with many dimples, as studied here, has about 33.8% more surface area (peripheral area) than a smooth surface. Thus, it can provide higher heat transfer from impinging jets compared to a smooth surface.

Figure 10 compares the Nusselt numbers between the many-dimples case and the many-pins case studied by Azad et al.[12] This study uses similar geometrical parameters, X/d, Y/d, and Z/d, and spent air crossflow orientations as used in Azad's study,[12] except the pinned target surface is replaced by a dimpled one. The dimples are made at same locations as of the pins. They are of same size and number. The dimpled surface Nusselt numbers for orientations 2 and 3 are about the same as for the pinned surface. The Nusselt numbers for the dimpled surface are slightly lower than the pinned surface for orientation 1. However, from application point of view, a dimpled surface is advantageous over a pinned surface. Pins increase material cost and add more weight to a surface, whereas dimples reduce material cost and weight. Thus, for applications such as internal cooling passage of a gas turbine blade, where material weight is an important factor, a dimpled surface may be an alternate option for enhancement of surface heat transfer rate. The designer should also consider that the dimples reduce wall thickness and may increase local stress. From heat transfer viewpoint, both dimpled and pinned surfaces are better than smooth surfaces if the increased surface area is taken into account.

The number of dimples (many or less as tested here) does have a positive influence on the heat transfer coefficient enhancement. The less-dimples case produces lower Nusselt number than the many-dimples case. Note that the data from the increased surface area due to the dimples (circumferential surface area), which is about 33.8% and 9% of the total projected surface area (for the many-dimples and the less-dimples cases, respectively), are not included in the calculation of the average heat transfer coefficient. The many-dimples case would provide even higher heat transfer compared to the less-dimples case due to its increased surface area. This study also provides a detailed measurement through the entire target surface.

Conclusion

The effect of a dimpled surface on local heat transfer coefficients for multiple jet impingement with three crossflow orientations is studied here. The local and averaged Nusselt numbers are measured. The results conclude the following.

1) Detailed measurement provides a better understanding of the jet impingement on a dimpled surface. These detailed heat transfer coefficient results also provide a reference for further experimental or computational study.

2) The jet Reynolds number has a strong effect on local heat transfer coefficient distribution. The local and the averaged Nusselt numbers increase with an increase in the jet Reynolds number.

3) For a smooth target surface, crossflow orientation 2 provides better heat transfer coefficient than orientation 1 and 3 (Ref. 7). Similarly, for a dimpled surface, crossflow orientation 2 also provides higher heat transfer coefficients than orientations 1 and 3.

4) The Nusselt numbers for a dimpled surface and a smooth surface are about the same. However, a dimpled surface provides higher heat transfer due to increased surface area (circumferential area), which is about 33.8 and 9% for our many-dimples and less-dimples cases, respectively.

5) The number of dimples does have a positive effect on heat transfer enhancement. The many-dimples case produces higher Nusselt numbers than the less-dimples case in this study. The many-dimples

case provides even higher heat transfer if the dimple increased circumferential area is considered, which is 33% in the many-dimples case compared to 9% in the less-dimples case.

6) The Nusselt numbers for a dimpled surface are about the same as for a pinned surface for spent air crossflow orientations 2 and 3, but lower for orientation 1. However, pins increase material cost and add weight to the surface, whereas dimples reduce both material cost and weight. A dimpled surface is as good as a pinned surface from an application point of view and provides an alternate option for enhancement of surface heat transfer for such applications as internal cooling passage of a gas turbine blade, where component weight is an important factor.

Acknowledgment

This work is supported by the Texas Higher Education Coordinating Board–Advanced Technology Program (Grant 999903-165).

References

[1]Kercher, D. M., and Tabakoff, W., "Heat Transfer by a Square Array of Round Air Jets Impinging Perpendicular to a Flat Surface Including the Effect of Spent Air," *Journal of Engineering and Power*, Vol. 92, No. 1, 1970, pp. 73–82.

[2]Florschuetz, L. W., Berry, R. A., and Metzger, D. E., "Periodic Streamwise Variation of Heat Transfer Coefficients for Inline and Staggered Arrays of Circular Jets with Crossflow of Spent Air," *Journal of Heat Transfer*, Vol. 102, No. 1, 1980, pp. 132–137.

[3]Chupp, R. E., Helms, H. E., McFadden, P. W., and Brown, T. R., "Evaluation of Internal Heat Transfer Coefficients for Impingement Cooled Turbine Blades," *Journal of Aircraft*, Vol. 6, No. 1, 1969, pp. 203–208.

[4]Bunker, R. S., and Metzger, D. E., "Local Heat Transfer in Internally Cooled Turbine Airfoil Leading Edge Regions: Part II—Impingement Cooling with Film Coolant Extraction," *Journal of Turbomachinery*, Vol. 112, No. 3, 1990, pp. 459–466.

[5]Metzger, D. E., and Bunker, R. S., "Local Heat Transfer in Internally Cooled Turbine Airfoil Leading Edge Regions: Part I—Impingement Cooling Without Film Coolant Extraction," *Journal of Turbomachinery*, Vol. 112, No. 3, 1990, pp. 451–458.

[6]Van Treuren, K. W., Wang, Z., Ireland, P. T., and Jones, T. V., "Detailed Measurements of Local Heat Transfer Coefficient and Adiabatic Wall Temperature Beneath an Array of Impingement Jets," *Journal of Turbomachinery*, Vol. 116, No. 2, 1994, pp. 369–374.

[7]Huang, Y., Ekkad, S. V., and Han, J. C., "Detailed Heat Transfer Distributions Under an Array of Orthogonal Impinging Jets," *Journal of Thermophysics and Heat Transfer*, Vol. 12, No. 1, 1998, pp. 73–79.

[8]Haiping, C., Dalin, Z., and Taiping, H., "Impingement Heat Transfer from Rib Roughened Surface Within Arrays of Circular Jet: The Effect of the Relative Position of the Jet Hole to the Ribs," American Society of Mechanical Engineers, Paper 97-GT-331, June 1997.

[9]Chakroun, W. M., Al-fahed, S. F., and Abdel-Rehman, A. A., "Heat Transfer Augmentation for Air Jet Impinged on Rough Surface," American Society of Mechanical Engineers, Paper 97-GT-436, June 1997.

[10]Trabold, T. A., and Obot, N. T., "Impingement Heat Transfer Within Arrays of Circular Jets. Part II: Effects of Crossflow in the Presence of Roughness Elements," American Society of Mechanical Engineers, Paper 87-GT-200, June 1987.

[11]Gau, C., and Lee, C. C., "Impingement Cooling Flow Structure and Heat Transfer Along Rib-Roughened Walls," *International Journal of Heat and Mass Transfer*, Vol. 35, No. 11, 1992, pp. 3009–3020.

[12]Azad, Gm. S., Huang, Y., and Han, J. C., "Jet Impingement Heat Transfer on Pinned Surfaces using a Transient Liquid Crystal Technique," 8th International Symposium on Transport Phenomena and Dynamics of Rotating Machinery, Honolulu, HI, March 2000.

[13]Chyu, M. K., Yu. Y., and Ding, H., "Concavity Enhanced Heat Transfer in an Internal Cooling Passage," American Society of Mechanical Engineers, Paper 97-GT-437, June 1997.

[14]Schukin, A. V., Kozlov, A. P., and Agachev, "Study and Application of Hemispherical Cavities for Surface Heat Transfer Augmentation," American Society of Mechanical Engineers, Paper 95-GT-59, June 1995.

[15]Afnasyev, V. N., Chudnovsky, Y. P., Leontiev, and Roganov, P. S., "Turbulent Flow Friction and Heat Transfer Characteristics for Spherical Cavities on a Flat Plate," *Experimental Thermal and Fluid Science*, Vol. 7, 1993, pp. 1–8.

[16]Terekov, V. I., Kalinina, S. V., and Mshvidobadze, Y. M., "Flow Structure and Heat Transfer on a Surface with a Unit Hole Depression," *Russian Journal of Engineering Thermophysics*, Vol. 5, 1995, pp. 11–34.

[17]Kline, S. J., and McClintock, F. A., "Describing Uncertainties in Single Sample Experiments," *Mechanical Engineering*, Vol. 75, No. 1, 1953, pp. 3–8.